Theory of Correlated Insulators and Superconductivity in Twisted Bilayer Graphene

Gal Shavit, Erez Berg, Ady Stern, and Yuval Oreg
Department of Condensed Matter Physics, Weizmann Institute of Science, Rehovot 76100, Israel

(Received 1 August 2021; accepted 18 November 2021; published 10 December 2021)

We introduce and analyze a model that sheds light on the interplay between correlated insulating states, superconductivity, and flavor-symmetry breaking in magic angle twisted bilayer graphene. Using a variational mean-field theory, we determine the normal-state phase diagram of our model as a function of the band filling. The model features robust insulators at even integer fillings, occasional weaker insulators at odd integer fillings, and a pattern of flavor-symmetry breaking at noninteger fillings. Adding a phonon-mediated intervalley retarded attractive interaction, we obtain strong-coupling superconducting domes, whose structure is in qualitative agreement with experiments. Our model elucidates how the intricate form of the interactions and the particle-hole asymmetry of the electronic structure determine the phase diagram. It also explains how subtle differences between devices may lead to the different behaviors observed experimentally. A similar model can be applied with minor modifications to other moiré systems, such as twisted trilayer graphene.

DOI: 10.1103/PhysRevLett.127.247703

Introduction.—When two graphene layers are stacked at a relative twist angle of $\sim 1.1°$, the lowest-lying electron bands become exceptionally flat [1]. Recently, this so-called magic angle twisted bilayer graphene (MATBG) emerged as a highly tunable platform to study strongly correlated physics. Correlated insulators (CIs), where interactions induce a gap and suppress transport, were first observed in MATBG at fillings of $\nu = \pm 2$ electrons per moiré unit cell relative to the charge neutrality point (CNP) [2,3]. Later experiments found a CI at $\nu = +3$ [4,5], and in some instances CIs were measured at nearly all integer fillings [6]. Empirically, insulating behavior is more pronounced for electrons ($\nu > 0$). The origin of these integer-filling CIs has been explored in several recent works [7–15].

Another remarkable feature of MATBG is the appearance of superconducting domes near the CIs at $\nu = \pm 2$ [3–5], with superconductivity generally being more robust for holes ($\nu < 0$), and (for both electrons and holes) on the $|\nu| > 2$ side. Experiments manipulating the electrostatic screening have indicated that Coulomb repulsion is either detrimental to superconductivity in MATBG or weakly affects it [4,5,16,17]. This suggests that electron-phonon coupling may play a role in MATBG [18–22], and plausibly induce superconductivity at certain fillings. However, the interplay between strong repulsion and its effect on the normal-state, retarded attraction due to phonons, and the unique multiband structure have yet to be fully explored.

In this Letter, we introduce and investigate a phenomenological model and find that it exhibits the most salient features of MATBG observed in experiments. The model comprises four electronic "flavors," accounting for spin and valley degeneracies, and interactions with strengths of the order of their bandwidth. The structure of the interaction terms and the features of the density of states (DOS) of noninteracting MATBG determine the phase diagram.

We find electron correlations induce CIs at even-integer fillings with intervalley coherent (IVC) order [i.e., spontaneously breaking valley $U_v(1)$ symmetry], whereas the odd-integer CIs, typically having bands with nonzero Chern numbers, are more sensitive to details of subleading interaction terms. At noninteger fillings, the system is not fully gapped, yet, the spin-valley flavor symmetry is broken [23–25]. Retarded intervalley attractive interactions, due to, e.g., phonons [19], then enable the formation of superconducting domes, which are most prominent at fillings which agree remarkably well with experiments. As depicted in Fig. 1, we recover a superconducting dome flanked by two insulators near $\nu = +2, +3$, and a more substantial dome on the hole-doped side of the $\nu = -2$ CI.

At certain fillings, strong-coupling superconductivity may be established, i.e., T_c becomes an appreciable fraction of the Fermi temperature T_F, leading to significant superconducting phase fluctuations, whose effect on transport we account for. This is enabled by the underlying normal state, where interactions induce spontaneous breaking of flavor-symmetry breaking *and* the valley $U_v(1)$ symmetries. Moreover, this symmetry-broken state has only two active flavors in different valleys and opposite spins, hence it may sustain large in-plane magnetic fields.

Model and results.—Our model comprises eight flat bands with valley (K/K'), spin, and sublattice (A/B) degrees of freedom, labeled by Pauli matrices τ_i, s_i, and σ_i, respectively. This basis is motivated by the MATBG sublattice-polarized basis discussed in Ref. [11]. These

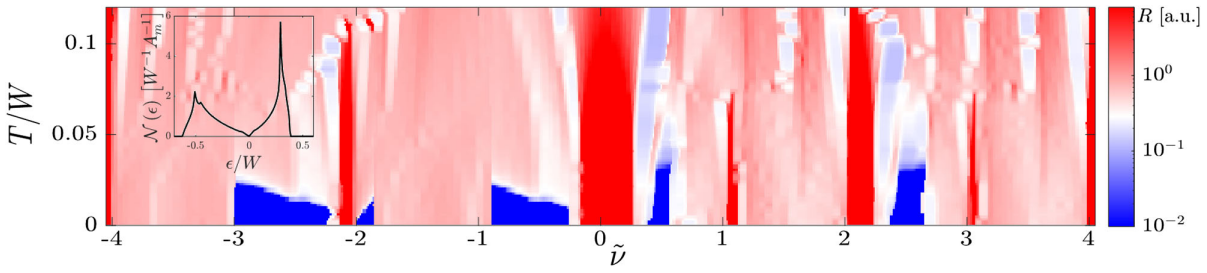

FIG. 1. Temperature and filling ($\tilde{\nu}$, see Supplemental Material [26], Sec. S3) phase diagram of the model. We plot the resistivity, inversely proportional to the compressibility far from the superconducting phase, see Supplemental Material [26], Sec. S5. The model features CIs near certain integer fillings and superconductivity, both in qualitative agreement with experiments. We used the interaction parameters [Eq. (3)] $U_C = 0.7W$, $U_\delta = 0.15W$, $g_1 = g_2 = 0.12W$, and phonon-mediated attraction strength [Eq. (6)] $V^* = 0.24W$. Inset: DOS of the single-particle Hamiltonian (2). For a detailed schematic phase diagram, and the effect of weaker Coulomb interactions, see Supplemental Material [26].

bands have a valley-dependent Chern number, $C = \tau_z\sigma_z$. The model Hamiltonian is

$$H = \sum_{\mathbf{k}} \Psi_{\mathbf{k}}^\dagger h_0(\mathbf{k}) \Psi_{\mathbf{k}} + H_{\text{int}}, \tag{1}$$

where H_{int} describes the interactions, $\Psi_{\mathbf{k}}$ is an 8-spinor of fermionic operators $c_{\tau s\sigma}(\mathbf{k})$ (annihilating an electron at valley τ, spin s and sublattice σ), and

$$h_0(\mathbf{k}) = f_x(\mathbf{k})\sigma_x + f_y(\mathbf{k})\sigma_y\tau_z + f_{p-h}(\mathbf{k}). \tag{2}$$

The functions f_x, f_y, and f_{p-h} determine the dispersion in the moiré Brillouin zone (mBZ), which has two Dirac cones with the same chirality, and reproduces an electronic DOS with the prominent features of the MATBG flat-bands (see Fig. 1 inset). Namely, linearly increasing DOS near the CNP, pronounced DOS peak near half-filling of the conduction or valence bands followed by a decline towards the band edge, and appreciable particle-hole asymmetry. The combined bandwidth of the conduction and valence bands in the mBZ is W. We note the form of $h_0(\mathbf{k})$ preserves $C_2 = \tau_x\sigma_x$ and time-reversal symmetries $\mathcal{T} = \tau_x\mathcal{K}$, with $\mathcal{K}$ the complex-conjugation operator [34]. For more about $h_0(\mathbf{k})$, see Supplemental Material, Sec. S1 [26].

We write electron-electron interactions as a sum of local interaction terms,

$$H_{\text{int}} = \sum_{\alpha,\mathbf{k},\mathbf{k}',\mathbf{q}} \frac{\lambda_\alpha}{2\Omega} (\Psi_{\mathbf{k}+\mathbf{q}}^\dagger \vec{\mathcal{O}}_\alpha \Psi_{\mathbf{k}}) \cdot (\Psi_{\mathbf{k}'-\mathbf{q}}^\dagger \vec{\mathcal{O}}_\alpha \Psi_{\mathbf{k}'}), \tag{3}$$

where Ω is the volume, $\vec{\mathcal{O}}_\alpha$ are matrices in valley-spin-sublattice space, and λ_α are coupling constants. The dominant term is the density-density interaction with $\vec{\mathcal{O}}_1 = \mathbb{1}$, $\lambda_1 = U_C$, and reflects the screened Coulomb repulsion. We consider a secondary interaction $\vec{\mathcal{O}}_2 = (\tau_z\sigma_x, \sigma_y)$ with $\lambda_2 = U_\delta$, accounting for the form factors obtained when projecting the Coulomb repulsion onto the flat-bands away from the chiral limit [11]. Additional terms are inspired by instantaneous interactions due to electron-optical-phonon interactions, $\vec{\mathcal{O}}_3 = (\sigma_y\tau_z, \sigma_x)$ with $\lambda_3 = g_1$, and $\vec{\mathcal{O}}_4 = (\tau_x\sigma_x, \tau_y\sigma_x)$ with $\lambda_4 = g_2$. Their structure is dictated by the electron-phonon coupling to low-momentum phonons ($\vec{\mathcal{O}}_3$) and to valley-momentum phonons ($\vec{\mathcal{O}}_4$) [18]. The phonon-induced interactions are attractive, i.e., g_1, $g_2 < 0$. The interactions preserve C_2, $\mathcal{T}$, and $C_3 = e^{2\pi i/3\sigma_z\tau_z}$ symmetries [35].

We study the model (1)–(3) using a variational Hartree-Fock approach. We minimize the grand-potential Φ, at a given temperature T and chemical potential μ, generated by the variational Hamiltonian $H_{\text{MF}} = \sum_{\mathbf{k}} \Psi_{\mathbf{k}}^\dagger h_{\text{MF}}(\mathbf{k}) \Psi_{\mathbf{k}}$ [26]. We note that in the mean-field approach, due to the local nature of the interactions, the details of the non-interacting dispersion do not play a role, only the DOS. We explore three kinds of spontaneous symmetry breaking in h_{MF}: (i) Flavor-symmetry breaking, i.e., one or several of the operators $\{s_z, \tau_z, \tau_z s_z\}$ attain a finite expectation value; (ii) intraflavor sublattice-symmetry breaking (σ_z terms), leading to Chern gaps; (iii) IVC order with a finite expectation value for $\tau_x \cos\gamma + \tau_y \sin\gamma$. We restrict our analysis to IVC terms of the form

$$\Delta_{\text{ivc}}^{\pm} \frac{1 \pm s_z\tau_z}{2} \tau_y s_x \sigma_y. \tag{4}$$

This order parameter resembles the Kramers-IVC of Ref. [11], with an effective time-reversal symmetry $\mathcal{T}' = \tau_y s_x \mathcal{K}$. The choice of $s_x\sigma_y$ in Eq. (4) is justified *a posteriori* by examination of the mean-field interaction energy (see Supplemental Material, Sec. S1 [26]). We find that the g_2 interaction favors orders where the spin is antialigned in opposite valleys, justifying s_x in Eq. (4). Moreover, we find U_δ and g_1 favor states where $\langle c_{\tau s\sigma}^\dagger c_{\bar{\tau}\,\bar{s}\,\bar{\sigma}}\rangle = -\langle c_{\tau s\bar{\sigma}}^\dagger c_{\bar{\tau}\,\bar{s}\,\sigma}\rangle^*$, so IVC orders $\propto \sigma_y$ gain interaction energy. Lastly, our analysis suggests sublattice-symmetry breaking is favored by g_1, yet *suppressed* by U_δ. The interplay between these interactions is key to

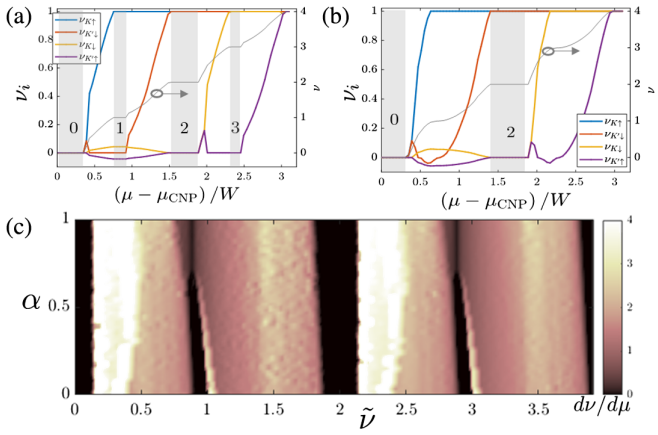

FIG. 2. (a) $T=0$ mean-field occupation ν_i of individual flavors and total filling ν as a function of chemical potential. Gray rectangles mark incompressible regions. Interaction parameters used: $U_C=0.75W$, $U_\delta=g_1=0.1W$, $g_2=0.08W$. (b) Same as (a), with $U_\delta=0.2W$ and $g_1=0$. (c) Compressibility $d\nu/d\mu$ as a function of $\tilde{\nu}$ and $\alpha\equiv[(U_\delta-g_1)/(U_\delta+g_1)]$, retaining $U_\delta+g_1=0.2W$, and all other parameters from (a)–(b). Notice (a) corresponds to $\alpha=0$ and (b) to $\alpha=1$.

understanding why insulators at odd fillings are experimentally less robust than those at even fillings.

Mean-field phase diagram results are displayed in Fig. 2. Panels (a)–(b) show the filling ν_i of each flavor for different values of U_δ and g_1. Our results feature a sequence of symmetry-breaking phase transitions. At the CNP, the system is in a fully gapped IVC state. With increased μ, the IVC gap in one $\tau_z s_z$ sector closes, and the two flavors making up that sector begin to populate [near $(\mu-\mu_{\mathrm{CNP}})/W\approx 0.4$ in Fig. 2]. This is followed by flavor-symmetry breaking within that sector, where one flavor is depleted and the other is filled. Depending on details, the depleted flavor may develop a Chern gap, leading to an incompressible region near $\nu=1$. Increasing μ further, this flavor is gradually filled. This process repeats for the flavors in the other IVC sector (starting at $\nu=2$), following an incompressible regime, where two flavors are full, and two others are IVC gapped.

We note that in a region around $\nu=1$, flavor polarization develops in the IVC sector, yet it remains incompressible. This is due to spin polarization in the more populated sector, promoting opposite polarization in opposing valleys, gaining interaction energy $\propto|g_2|$.

In Fig. 2(c) we plot the compressibility $d\nu/d\mu$ as a function of $\alpha\equiv[(U_\delta-g_1)/(U_\delta+g_1)]$ and $\tilde{\nu}$. The latter is a proxy for the filling fraction representing the experimental scenario, where a back-gate voltage tunes the electron filling, see Supplemental Material, Sec. S3 [26]. As α increases, (g_1 becomes smaller compared to U_δ) the odd-filling gaps close and eventually vanish at $\alpha\sim 0.7$, giving way to finite but low compressibility [24]. This trend agrees with our analytical examination of the roles of U_δ and g_1. The $\tilde{\nu}=0,2$ incompressible IVC states weakly depend on α, and thus expected to be more robust.

The phase diagram establishes that the appearance of CIs either at all integer fillings, or only at even ones, depends delicately on the details and hierarchy of the effective interaction terms [36]. We note that the appearance of σ_y–IVC orders at even fillings agrees with the predictions of Ref. [11] and was verified numerically [39]. This is expected as the U_δ term captures the effect of the density form-factors of the projected interaction. Our model thus provides a tractable way of going beyond specific integer fillings and tracking the evolution of the mean-field ground state with μ.

Superconductivity.—Our starting point of examining superconductivity in MATBG is the symmetry-breaking cascade obtained above. We explore intervalley pairing mediated by electron-phonon interactions. The intervalley pairing is favored both by the acoustic phonons [19] and since intravalley Cooper pairs have finite momentum. Thus, we focus on valley-degenerate areas in the phase diagram. We note that scenarios where the superconducting condensation energy gain is sufficient to depolarize opposite-valley flavors are not considered.

As discussed, the model favors intervalley antiferromagnetism, naturally preferring opposite-spin pairing. Restricting our discussion to the simplest scenario where the pairing lacks sublattice structure (it is sufficient to capture the most salient experimental features), we study the pairing amplitude $\Delta_{\tau s}=\Delta_{\tau sA}=\Delta_{\tau sB}$, where

$$\Delta_{\tau s\sigma}=\frac{1}{\Omega}\sum_{\mathbf{k}}\langle c_{\bar{\tau}\bar{s}\sigma}(-\mathbf{k})c_{\tau s\sigma}(\mathbf{k})\rangle. \tag{5}$$

We note that due to the aforementioned spontaneous spin-valley locking and flavor-symmetry breaking, the system attains nonzero spin-triplet pairing correlations [40]. This may lead to phenomenology similar to that of Ising superconductors, namely, a critical in-plane magnetic field that is set by the normal-state energetics, exceeding the Pauli-Chandrasekhar-Clogston limit [41–43].

Adopting a Tolmachev-Morel-Anderson renormalization group (RG) approach [44,45], we account for the effects of Coulomb repulsion as well as the phonon-mediated attraction. Neglecting the attraction for now, we begin with the action $\mathcal{S}=\mathcal{S}_{\mathrm{MF}}+\mathcal{S}_{\mathrm{Cooper}}$, where S_{MF} is corresponds to the solution of the variational procedure, and $\mathcal{S}_{\mathrm{Cooper}}=\int d^2\mathbf{x}\sum_{\tau s\sigma}c^\dagger_{\tau s\sigma}c^\dagger_{\bar{\tau}\bar{s}\sigma}[(U_C/2)c_{\bar{\tau}\bar{s}\sigma}c_{\tau s\sigma}-(U_\delta+|g_1|)c_{\bar{\tau}\bar{s}\bar{\sigma}}c_{\tau s\bar{\sigma}}]$ is the interaction in the $\Delta_{\tau s}$ Cooper channel. Following the standard RG procedure [26,46], we find the flow of the coupling constant V as a function of the energy cutoff Λ. The initial conditions are $\Lambda_0=W$, and $V_0=(U_C/2)-(U_\delta+|g_1|)$. Notice the secondary interactions *enhance* pairing whereas Coulomb repulsion suppresses it.

We now address the role of the acoustic phonon branch mediating the retarded attraction. We observe that due to folding of the phonon spectrum into the mBZ [47,48], one should also consider generated "pseudo-optical" branches. Consequently, the RG equation for the coupling constant is [26]

$$\frac{d}{d\Lambda}V = \frac{\mathcal{N}(\Lambda)}{\Lambda}V^2 + \frac{V^*}{W}, \tag{6}$$

where the conventional RG flow yields the first term, with $\mathcal{N}(\Lambda)$ the electronic DOS. The nonstandard second term appears because as one lowers the cutoff, more phonon modes become attractive, we denote their total contribution by V^*, see Supplemental Material [26], Sec. S4.

Using Eq. (6), in conjunction with the mean-field results, we find T_c, extracted as the scale at which the coupling constant becomes comparable with the bandwidth, $|V(T_c)| = W$, signaling its divergence. Notice because W is the scale at which retarded phonons begin contributing, at a given V^* and V_0, Eq. (6) may lead to a critical W, *below which* superconductivity is lost. This is due to the retardation being ineffective in changing the sign of V along the shorter RG flow. Figure 3 tracks the evolution of superconductivity domes with increasing phonon-mediated attraction V^*.

To take into account the effects of superconducting phase fluctuations on transport, which may be significant as T_c and T_F become comparable, we use the Halperin-Nelson formula to calculate the resistivity (Supplemental Material, Sec. S5 [26,49]). The difference between the mean-field T_c and the BKT temperature can be parametrized by $T_{\mathrm{BKT}} = T_c/(1+\tau_c)$, where $\tau_c \approx T_c/T_F$. Experimental estimates [3] of $\tau_c \sim 0.05$–0.1 in MATBG are in qualitative agreement with the values obtained for T_c and T_F with our model, where we find τ_c in a similar range on the hole side of Fig. 1, and τ_c reaching up to ∼0.3 on the electron side.

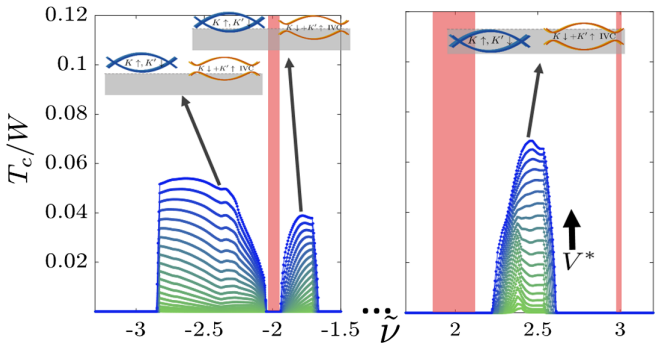

FIG. 3. Superconducting T_c enhancement with increasing retarded attraction V^* near representative fillings. We used the parameters of Fig. 1, with $V^* \in [0.12, 0.32]W$, in steps of 0.01 W. Red: incompressibility regions. Direction of increased V^* is indicated, as are the schematic mean-field states from which superconductivity emerges.

Nonzero normal-state $\Delta_{\mathrm{ivc}}^{\pm}$ modifies the dispersion, enabling an appreciable Fermi-level DOS even at minuscule fillings. It thus contributes to increasing T_c/T_F as compared to what is expected from a Dirac-like dispersion.

Figure 1 features three superconducting domes on the hole side. The most prominent one occurs at $\tilde{\nu} = -2-\epsilon$, bordering the $\tilde{\nu} = -2$ IVC phase. Here, the gap in the IVC sector gradually closes with decreasing $\tilde{\nu}$, until it vanishes. The suppression in superconductivity near $\tilde{\nu} \approx -3$ occurs due to flavor polarization, similar to those shown in Fig. 2. Superconductivity at this filling is the most experimentally robust, often observed with similar double-hump shape [3]. This shape is due to the two-step process, where first the IVC gap closes with doping, and then two gapless flavors get populated. A similar, but narrower and higher dome emerges at $\tilde{\nu} = 2+\epsilon$. This is because the electron side has larger DOS leading to stronger effective repulsion and wider regions with flavor polarization. On the other hand, without polarization the larger DOS leads to higher T_c.

A secondary superconducting feature observed in some experiments appears near $|\nu| = 2-\epsilon$, and is also manifest in our model at $\tilde{\nu} = -2+\epsilon$. Its existence is due to depolarization of the two non-IVC flavors when $\tilde{\nu}$ is decreased (see Supplemental Material, [26], Fig. S1), resulting from the drop in DOS near the band edge. Thus, this feature is sensitive to the flat-band dispersion details, possibly explaining its haphazard occurrence.

Lastly, we find superconductivity near the CNP, seldom observed in experiments [6]. Essentially, it is a modified copy of the $\tilde{\nu} = -2-\epsilon$ dome, with two flavors facilitating the pairing, and two forming a gapped-IVC state. It has an electron-side counterpart, too.

Discussion.—We presented a simple phenomenological model unifying key features of MATBG, namely, interaction-induced CIs at integer fillings, flavor-symmetry-breaking phase transitions, and nonstandard superconductivity, and demonstrating their interplay. Though we neglect ingredients known to be found in MATBG, i.e., long-range Coulomb interactions, intricate wave functions, fragile topology, and filling-dependent band structure, much of the phenomenology is remarkably reproduced. Our minimalistic description of the system's degrees of freedom, and the hierarchy of the interaction energy scales, help to comprehend the experimental phase diagram and its variations between different devices.

The model incorporates two important effects of the twist-induced moiré lattice. First, generation of a flat-band dispersion, with greatly enhanced DOS [1]. Second, a dramatic increase of the electron-phonon coupling [19]. The large DOS enhances the effects of both electron-electron repulsion and the effective phonon-mediated attraction. Here, we use a mean-field approach combined with RG method to study the interplay of the two. Within this paradigm, one expects that the CIs and

superconductivity compete with one another. This is consistent with experiments where the strength of the Coulomb interaction is tuned by manipulating the screening environment [5,16,17]. Another side effect of this interplay is spontaneous spin-valley locking, e.g., near $\nu = -2 - \epsilon$, that may be weakly sensitive to parallel in-plane magnetic fields, leading to a superconducting order parameter with appreciable spin-triplet pairing correlations.

It is worth noting the discrepancies between our simplified model and experimental observations. In most experiments, the CNP phase appears semimetallic (though there are notable exceptions). Here, we find the strongest CI at this filling. Furthermore, we find that a $|\nu| = 3$ insulator is accompanied by an insulator at $|\nu| = 1$, seldom seen in experiments. One possible cause is a modification of the band structure itself the filling changes. It has been argued [50–53] that the flat bands are least flat near charge neutrality, which may explain the empirical scarcity of insulators at low fillings. Another possibility is that the semimetal at the CNP is promoted by strain [54]. These effects are not considered in this work. Moreover, there is convincing experimental evidence [55,56] that flavor fluctuations near $|\nu| = 1$ are non-negligible, suggesting one should include spin and valley fluctuations to fully understand this regime.

Disorder was also not explored in this model. As was suggested [57], it may settle the discrepancy regarding the CNP insulator, as well as the absence of a quantized transverse response at odd fillings CIs. Our proposed framework can help elucidate the roles of both fluctuations (treating our phase diagram as a saddle point around which fluctuations occur) and disorder (quantifying the competition between phases and accounting for how disorder affects it).

Our model may be used to investigate additional superconducting channels, e.g., d wave [18], and explore under what conditions they become dominant. Furthermore, this scheme, with different interactions, single-particle terms, or DOS, may apply to other moiré platforms displaying correlation-induced phenomena, e.g., ABC-stacked trilayer graphene on hexagonal boron-nitride (hBN) [58], twisted double-bilayer graphene [59,60], MATBG aligned with hBN [61,62] (where we may explain the absence of superconductivity, Supplemental Material [26], Sec. S6), and magic-angle twisted trilayer graphene [63,64].

We acknowledge enlightening discussions with Pablo Jarillo-Herrero, Shahal Ilani, Uri Zondiner, Ohad Antebi, and Keshav Pareek. This project was partially supported by grants from the ERC under the European Union's Horizon 2020 research and innovation programme (Grant Agreements LEGOTOP No. 788715 and HQMAT No. 817799), the DFG (CRC/Transregio 183, EI 519/7-1), the BSF and NSF (2018643), the ISF Quantum Science and Technology (2074/19), and a research grant from Irving and Cherna Moskowitz.

[1] R. Bistritzer and A. H. MacDonald, Proc. Natl. Acad. Sci. U.S.A. **108**, 12233 (2011).
[2] Y. Cao, V. Fatemi, A. Demir, S. Fang, S. L. Tomarken, J. Y. Luo, J. D. Sanchez-Yamagishi, K. Watanabe, T. Taniguchi, E. Kaxiras, R. C. Ashoori, and P. Jarillo-Herrero, Nature (London) **556**, 80 (2018).
[3] Y. Cao, V. Fatemi, S. Fang, K. Watanabe, T. Taniguchi, E. Kaxiras, and P. Jarillo-Herrero, Nature (London) **556**, 43 (2018).
[4] M. Yankowitz, S. Chen, H. Polshyn, Y. Zhang, K. Watanabe, T. Taniguchi, D. Graf, A. F. Young, and C. R. Dean, Science **363**, 1059 (2019).
[5] Y. Saito, J. Ge, K. Watanabe, T. Taniguchi, and A. F. Young, Nat. Phys. **16**, 926 (2020).
[6] X. Lu, P. Stepanov, W. Yang, M. Xie, M. A. Aamir, I. Das, C. Urgell, K. Watanabe, T. Taniguchi, G. Zhang, A. Bachtold, A. H. MacDonald, and D. K. Efetov, Nature (London) **574**, 653 (2019).
[7] H. C. Po, L. Zou, A. Vishwanath, and T. Senthil, Phys. Rev. X **8**, 031089 (2018).
[8] J. F. Dodaro, S. A. Kivelson, Y. Schattner, X. Q. Sun, and C. Wang, Phys. Rev. B **98**, 075154 (2018).
[9] J. Kang and O. Vafek, Phys. Rev. Lett. **122**, 246401 (2019).
[10] K. Seo, V. N. Kotov, and B. Uchoa, Phys. Rev. Lett. **122**, 246402 (2019).
[11] N. Bultinck, E. Khalaf, S. Liu, S. Chatterjee, A. Vishwanath, and M. P. Zaletel, Phys. Rev. X **10**, 031034 (2020).
[12] J. Kang and O. Vafek, Phys. Rev. B **102**, 035161 (2020).
[13] O. Vafek and J. Kang, Phys. Rev. Lett. **125**, 257602 (2020).
[14] B. Lian, Z.-D. Song, N. Regnault, D. K. Efetov, A. Yazdani, and B. A. Bernevig, Phys. Rev. B **103**, 205414 (2021).
[15] F. Xie, A. Cowsik, Z.-D. Song, B. Lian, B. A. Bernevig, and N. Regnault, Phys. Rev. B **103**, 205416 (2021).
[16] P. Stepanov, I. Das, X. Lu, A. Fahimniya, K. Watanabe, T. Taniguchi, F. H. L. Koppens, J. Lischner, L. Levitov, and D. K. Efetov, Nature (London) **583**, 375 (2020).
[17] X. Liu, Z. Wang, K. Watanabe, T. Taniguchi, O. Vafek, and J. I. A. Li, Science **371**, 1261 (2021).
[18] F. Wu, A. H. MacDonald, and I. Martin, Phys. Rev. Lett. **121**, 257001 (2018).
[19] B. Lian, Z. Wang, and B. A. Bernevig, Phys. Rev. Lett. **122**, 257002 (2019).
[20] F. Wu, E. Hwang, and S. Das Sarma, Phys. Rev. B **99**, 165112 (2019).
[21] B. A. Bernevig, B. Lian, A. Cowsik, F. Xie, N. Regnault, and Z.-D. Song, Phys. Rev. B **103**, 205415 (2021).
[22] C. Lewandowski, D. Chowdhury, and J. Ruhman, Phys. Rev. B **103**, 235401 (2021).
[23] D. Wong, K. P. Nuckolls, M. Oh, B. Lian, Y. Xie, S. Jeon, K. Watanabe, T. Taniguchi, B. A. Bernevig, and A. Yazdani, Nature (London) **582**, 198 (2020).
[24] U. Zondiner, A. Rozen, D. Rodan-Legrain, Y. Cao, R. Queiroz, T. Taniguchi, K. Watanabe, Y. Oreg, F. von Oppen, A. Stern, E. Berg, P. Jarillo-Herrero, and S. Ilani, Nature (London) **582**, 203 (2020).
[25] J. Kang, B. A. Bernevig, and O. Vafek, arXiv:2104.01145.
[26] See Supplemental Material at http://link.aps.org/supplemental/10.1103/PhysRevLett.127.247703 for details regarding the single-particle Hamiltonian, the variational

mean-field approach, calculation of $\tilde{\nu}$, the superconducting RG equation, the role of superconducting phase fluctuations, the effect of electrostatic screening, estimation of relevant coupling constants, and suppression of superconductivity by alignment with h-BN, which includes Refs. [27–33].
[27] P. B. Allen and R. C. Dynes, Phys. Rev. B **12**, 905 (1975).
[28] N. B. Kopnin and E. B. Sonin, Phys. Rev. Lett. **100**, 246808 (2008).
[29] A. Abrikosov, *Fundamentals of the Theory of Metals* (Dover Publications, New York, 2017).
[30] L. Aslamasov and A. Larkin, Phys. Lett. **26A**, 238 (1968).
[31] H. Kim, N. Leconte, B. L. Chittari, K. Watanabe, T. Taniguchi, A. H. MacDonald, J. Jung, and S. Jung, Nano Lett. **18**, 7732 (2018).
[32] H. Akera, A. H. MacDonald, S. M. Girvin, and M. R. Norman, Phys. Rev. Lett. **67**, 2375 (1991).
[33] K. Maki, in *Superconductivity: Part 2* (CRC Press, Boca Raton, 1969), pp. 1035–1105.
[34] The single-particle term in the Hamiltonian we use is not C_3 symmetric, unlike the MATBG dispersion. However, within this model it has little consequence, as we also do not explore spontaneous C_3-symmetry breaking.
[35] It can be directly checked, for example, that $(\Psi^\dagger C_3 \vec{\mathcal{O}}_\alpha C_3^\dagger \Psi)^2 = (\Psi^\dagger \vec{\mathcal{O}}_\alpha \Psi)$ for $\alpha = 1, \ldots, 4$.
[36] This sensitivity is a common feature in quantum Hall ferromagnets [37,38], whose physics which is arguably pertinent to the theory of MATBG.
[37] K. Nomura and A. H. MacDonald, Phys. Rev. Lett. **96**, 256602 (2006).
[38] M. Kharitonov, Phys. Rev. B **85**, 155439 (2012).
[39] J. S. Hofmann, E. Khalaf, A. Vishwanath, E. Berg, and J. Y. Lee, arXiv:2105.12112.
[40] B. T. Zhou, N. F. Q. Yuan, H.-L. Jiang, and K. T. Law, Phys. Rev. B **93**, 180501(R) (2016).
[41] A. M. Clogston, Phys. Rev. Lett. **9**, 266 (1962).
[42] J. M. Lu, O. Zheliuk, I. Leermakers, N. F. Q. Yuan, U. Zeitler, K. T. Law, and J. T. Ye, Science **350**, 1353 (2015).
[43] X. Xi, Z. Wang, W. Zhao, J.-H. Park, K. T. Law, H. Berger, L. Forró, J. Shan, and K. F. Mak, Nat. Phys. **12**, 139 (2016).
[44] V. V. Tolmachev, Dokl. Akad. Nauk SSSR **140**, 563 (1961), http://mi.mathnet.ru/dan25552
[45] P. Morel and P. W. Anderson, Phys. Rev. **125**, 1263 (1962).
[46] N. Nagaosa, *Quantum Field Theory in Condensed Matter Physics* (Springer Science & Business Media, New York, 1999).
[47] T. Cea and F. Guinea, Proc. Natl. Acad. Sci. U.S.A. **118**, e2107874118 (2021).
[48] A. I. Cocemasov, D. L. Nika, and A. A. Balandin, Phys. Rev. B **88**, 035428 (2013).
[49] B. I. Halperin and D. R. Nelson, J. Low Temp. Phys. **36**, 599 (1979).
[50] M. J. Calderón and E. Bascones, Phys. Rev. B **102**, 155149 (2020).
[51] Z. A. H. Goodwin, V. Vitale, X. Liang, A. A. Mostofi, and J. Lischner, arXiv:2004.14784.
[52] M. Xie and A. H. MacDonald, Phys. Rev. Lett. **127**, 196401 (2021).
[53] C. Lewandowski, S. Nadj-Perge, and D. Chowdhury, npj Quantum Mater. **6**, 82 (2021).
[54] D. E. Parker, T. Soejima, J. Hauschild, M. P. Zaletel, and N. Bultinck, Phys. Rev. Lett. **127**, 027601 (2021).
[55] Y. Saito, F. Yang, J. Ge, X. Liu, K. Watanabe, T. Taniguchi, J. I. A. Li, E. Berg, and A. F. Young, Nature (London) **592**, 220 (2021).
[56] A. Rozen, J. M. Park, U. Zondiner, Y. Cao, D. Rodan-Legrain, T. Taniguchi, K. Watanabe, Y. Oreg, A. Stern, E. Berg, P. Jarillo-Herrero, and S. Ilani, Nature (London) **592**, 214 (2021).
[57] A. Thomson and J. Alicea, Phys. Rev. B **103**, 125138 (2021).
[58] G. Chen, L. Jiang, S. Wu, B. Lyu, H. Li, B. L. Chittari, K. Watanabe, T. Taniguchi, Z. Shi, J. Jung, Y. Zhang, and F. Wang, Nat. Phys. **15**, 237 (2019).
[59] M. He, Y. Li, J. Cai, Y. Liu, K. Watanabe, T. Taniguchi, X. Xu, and M. Yankowitz, Nat. Phys. **17**, 26 (2021).
[60] C. Shen, Y. Chu, Q. Wu, N. Li, S. Wang, Y. Zhao, J. Tang, J. Liu, J. Tian, K. Watanabe, T. Taniguchi, R. Yang, Z. Y. Meng, D. Shi, O. V. Yazyev, and G. Zhang, Nat. Phys. **16**, 520 (2020).
[61] G. Chen, A. L. Sharpe, E. J. Fox, Y.-H. Zhang, S. Wang, L. Jiang, B. Lyu, H. Li, K. Watanabe, T. Taniguchi, Z. Shi, T. Senthil, D. Goldhaber-Gordon, Y. Zhang, and F. Wang, Nature (London) **579**, 56 (2020).
[62] M. Serlin, C. L. Tschirhart, H. Polshyn, Y. Zhang, J. Zhu, K. Watanabe, T. Taniguchi, L. Balents, and A. F. Young, Science **367**, 900 (2020).
[63] J. M. Park, Y. Cao, K. Watanabe, T. Taniguchi, and P. Jarillo-Herrero, Nature (London) **590**, 249 (2021).
[64] Z. Hao, A. M. Zimmerman, P. Ledwith, E. Khalaf, D. H. Najafabadi, K. Watanabe, T. Taniguchi, A. Vishwanath, and P. Kim, Science **371**, 1133 (2021).